Optics Letters

Low voltage blue phase liquid crystal for spatial light modulators

FENGLIN PENG, YUN-HAN LEE, ZHENYUE LUO, AND SHIN-TSON WU*

CREOL, The College of Optics and Photonics, University of Central Florida, Orlando, Florida 32816, USA
*Corresponding author: swu@ucf.edu

Received 2 September 2015; revised 5 October 2015; accepted 5 October 2015; posted 8 October 2015 (Doc. ID 249321); published 30 October 2015

We demonstrated a low-voltage polymer-stabilized blue phase liquid crystal (BPLC) for phase-only modulation with a liquid-crystal-on-silicon (LCoS). A new device configuration was developed, which allows the incident laser beam to traverse the BPLC layer four times before exiting the LCoS. As a result, the 2π phase change voltage is reduced to below 24 V in the visible region. The response time remains relatively fast (~3 ms). The proposed device configuration enables widespread applications of BPLC spatial light modulators.

OCIS codes: (160.3710) Liquid crystals; (230.3720) Liquid-crystal devices; (120.5060) Phase modulation.

http://dx.doi.org/10.1364/OL.40.005097

A liquid crystal spatial light modulator (LC-SLM) [1] is a useful electro-optic device for modulating the phase of an incident light. Its applications include adaptive optics [2], adaptive lens [3], laser beam control [4–7], phase gratings [8], and quantum information science [9]. For phase modulation, low operation voltage for 2π phase change ($V_{2\pi}$) and fast response time are two critical requirements. An SLM using nematic LC has advantages in low $V_{2\pi}$; however, its response time is relatively slow, typically 30–100 ms depending on the LC layer thickness employed [10]. To achieve fast response time, polymer network liquid crystal (PNLC) has been developed for infrared SLM [11,12], where light scattering is negligible. However, to extend PNLC to be visible with suppressed scattering, the domain size should be <200 nm [13] which, in turn, increases $V_{2\pi}$ dramatically. Polymer-stabilized blue phase liquid crystal (PS-BPLC) [14] is another promising candidate for photonics and display applications [8]. However, its $V_{2\pi}$ is also relatively high.

In terms of device, liquid-crystal-on-silicon (LCoS) is a commonly used reflective SLM because of its high resolution and simple fabrication process [10]. In the past, BPLC-based LCoS has been demonstrated for intensity [15] and phase [16] modulations. For phase modulation, 2π modulo is generally required. Two problems contributing to high $V_{2\pi}$ are the small Kerr constant (K) of the employed LC host and that the refractive index change (δn) is only one-third of the induced birefringence (Δn_{ind}) under longitudinal electric field condition:

$$\delta n = \frac{\Delta n_{\text{ind}}(E)}{3} = n_i - n_o(E). \quad (1)$$

In Eq. (1), n_i represents the optically isotropic refractive index at the voltage-off state ($V = 0$), $n_o(E)$ is the induced ordinary refractive index, and E is the electric field. The maximum induced birefringence is proportional to the intrinsic birefringence of the LC host. The total phase change (δ) is jointly determined by the optical path length (l) of the SLM, δn, and operating wavelength (λ) as

$$\delta = 2\pi l(\delta n)/\lambda. \quad (2)$$

The optical path length is linearly proportional to the cell gap (d) as

$$l = Ad. \quad (3)$$

Here, A is a parameter related to device configuration, e.g., $A = 1$ for transmissive SLM and $A = 2$ for reflective LCoS. From Eq. (2), to achieve $\delta = 2\pi$, the minimal cell gap for an LCoS is $d = \lambda/(2\delta n)$. Let us assume $\lambda = 633$ nm and $\Delta n_{\text{ind}} \sim 0.1$ at ~4 V/μm for the employed PS-BPLC; then the required cell gap is $d \sim 10$ μm. For such a thick cell gap, we find $V_{2\pi} \sim 40$ V, which exceeds the maximum affordable voltage (24 V) of a high-resolution LCoS [17]. To keep $V_{2\pi}$ below 24 V, large birefringence and new device configuration with $A > 2$ are highly desirable. From a materials aspect, a BPLC with a large Kerr constant is useful because the on-state voltage is inversely proportional to $\sqrt{K}$ [18]. From an optics viewpoint, it is critical to boost the optical path length (i.e., large A) while keeping a thin cell gap (for low voltage). Therefore, to integrate BPLC into LCoS for widespread applications, there is an urgent need to develop a new device structure with $V_{2\pi} < 24$ V.

In this Letter, we demonstrate a low-voltage polymer-stabilized BPLC for LCoS applications. A new device configuration is developed, which allows the incoming laser beam to traverse four times inside the BPLC layer before exiting the cavity. Such an optical system doubles the phase change over conventional LCoS.

Figure 1 depicts the device configuration and operation mechanism of the proposed LCoS SLM. The PS-BPLC is sandwiched between pixelated reflective aluminum (Al) electrodes and a common ITO (indium tin oxide) electrode. No PI layer is needed for both substrates. At $V = 0$, the PS-BPLC is optically isotropic, and the corresponding refractive index is n_i. As a longitudinal electric field (along z axis) is applied, the LC directors are reoriented along the electric field direction because the host

nematic LC has a positive dielectric anisotropic ($\Delta\varepsilon > 0$). As a result, the optical axis of the induced refractive index ellipsoid elongates with the electric field. Therefore, both TE and TM polarizations experience the ordinary refractive index n_o, and the induced birefringence ($n_i - n_o$) is polarization independent for the normally incident light. To increase the optical path length in order to accumulate a larger phase change, we place a reflective polarizer {e.g., wire grid polarizer or DBEF (dual brightness enhancement film) [19]} on top of the glass substrate, as Fig. 1 shows. For the convenience of discussion, here we assume that the reflective polarizer reflects the TE mode (i.e., s-wave) and transmits TM (p-wave), and the incident collimated linearly polarized laser beam is in TM mode. In addition, a broadband quarter-wave ($\lambda/4$) plate is laminated between the reflective polarizer and the ITO glass substrate. The axis of $\lambda/4$ plate is 45° with respect to that of a reflective polarizer. After passing through the $\lambda/4$ plate, the TM wave turns to right-hand circular polarization (e.g., first RCP). When it traverses the BPLC layer once, it experiences the same phase accumulation in both x and y directions as shown in Fig. 1. Upon reflection from the Al electrode, the polarization remains circular but, with an opposite handedness, shown as second LCP (left-hand circular polarization). As the light passes through the $\lambda/4$ plate the second time, the original TM wave is changed to TE so that it is reflected by the reflective polarizer. Then it passes through the $\lambda/4$ plate the third time and enters the BPLC layer as the third LCP. Similarly, the light is reflected by the Al mirror and traverses the BPLC layer (fourth RCP) and the $\lambda/4$ plate for the fourth time. The polarization state returns to TM so that the light transmits through the reflective polarizer. Therefore, the optical path length is accumulated fourfold. This makes the following important impact: if we want to obtain 2π phase change, then the cell gap can be reduced by 2×, as compared to conventional LCoS. As a result, the required operation voltage is reduced. Moreover, the fringing field effect of a high-resolution LCoS can be suppressed for two important reasons: thinner cell gap and circularly polarized light inside the BPLC layer [20,21]. Besides PS-BPLC, any optically isotropic LC material (e.g., nano-sized polymer-dispersed liquid crystal [22]) can also be applied in the proposed device configuration.

For some applications, the input light could be at an off-axis angle. Such an incident light experiences different refractive index in the quarter-wave plate, as well as a BPLC layer at an on-state voltage, and the circular polarized light turns to elliptical. Therefore, the light cannot be fully turned into TM mode in the fourth path, resulting in some intensity loss. The reflective polarizer works well for the incident light at an oblique angle [19]. We investigated the oblique angle effect using a commercial LCD simulator DIMOS 2.0. In simulation, we set the operation wavelength at $\lambda = 550$ nm and employed a linearly polarized light. The PS-BBLC in the voltage-on state is assumed to have $\Delta n_{\text{ind}} \sim 0.1$ and can be regarded as a vertically aligned nematic layer. When the incident angle changes within ±10°, the reflectance difference is less than 5%. In comparison with reflective polarizer or DBEF, the phase retardation in the BPLC layer is relatively small and can be ignored. However, a large oblique angle incidence could induce a noticeable lateral shift for the outgoing beam, which leads to crosstalk in a high-resolution LCoS.

In the experiment, we prepared a PS-BPLC sample employing JC-BP07N (from JNC, Japan) as a nematic LC host. The dielectric anisotropy ($\Delta\varepsilon$) at low frequency ($f = 300$ Hz) is ~332. The PS-BPLC precursor is composed of 87.99 wt. % JC-BP07N, 2.84 wt. % chiral dopant R5011 (from HCCH, China), 5.42 wt. % RM257 (from Merck), and 3.74 wt. % TMPTA (1,1,1-trimethylolpropane triacrylate, from Sigma-Aldrich). The sample was filled into a vertical field switching (VFS) cell [23] with cell gap $d \sim 4.97$ μm. Both substrates were coated with ITO electrodes, but without any surface alignment layers. The cell was cooled to the BP-I phase and cured by UV light with $\lambda \sim 365$ nm and intensity ~8 mW/cm^2 for 15 min. After UV curing, the PS-BPLC cell was quite clear since its Bragg reflection is in the UV region. For convenience, we call it PS-BPLC07. To investigate the electro-optic performance of proposed PS-BPLC spatial light modulator, we used Michelson interferometer, as Fig. 2 depicts. The light source was an unpolarized He-Ne laser ($\lambda = 633$ nm), and it turned to be linearly polarized light after polarizer 1. The linearly polarized light was split equally into two arms by the beam splitter (BS). The phase modulation arm worked as the proposed PS-BPLC LCoS spatial light modulator (Fig. 1) with a single pixel. Since the DBEF for display applications is usually combined with an embossed front surface and will diffuse the incident laser light, it is replaced by a polarizing beam splitter (PBS) and a mirror in the experimental setup. The incident light was along with the transmission axis of PBS. The PS-BPLC sample was sandwiched between a quarter-wave plate at $\lambda = 633$ nm and a reflective mirror. The sample was driven by a square-wave voltage with frequency $f = 100$ Hz [24]. Fringes were observed and recorded by a CMOS camera (DCC1545M, Thorlab). Through the average measured light intensity change under applied voltage, we obtained the induced phase change. In the reference arm, we put two polarizers to adjust the light intensity and improve the contrast of fringes, because more light loss exists in the phase modulation arm due to multi-surface reflection of optical components.

In Fig. 3(a), black dots represent the experimental data of the voltage dependent phase change for PS-BPLC07. In the

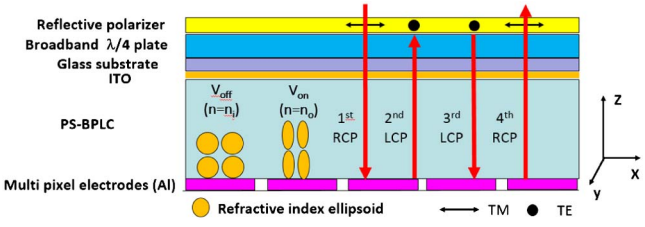

Fig. 1. Proposed device configuration of BPLC-based LCoS SLM.

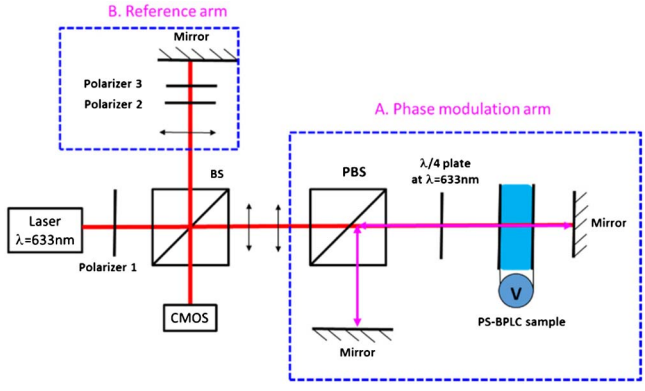

Fig. 2. Experimental setup for measuring the phase change.

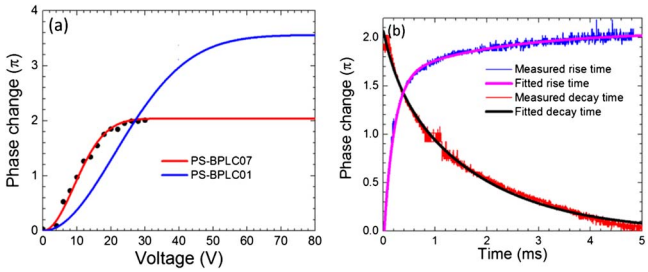

Fig. 3. (a) Voltage dependent phase change of PS-BPLC07 and PS-BPLC01. Black dots are the experimental data; based on Eq. (5); red and blue lines stand for the fitting and simulated curves, respectively. (b) Measured phase rise and decay times of PS-BPLC07 and corresponding fitting curve with double exponential equations.

voltage-off state, the PS-BPLC is optically isotropic with refractive index n_i, and we set it as reference point, i.e., there is no phase change at $V = 0$. As the applied voltage increases, the phase change increases rapidly and then saturates gradually. As shown in Fig. 3(a), the phase change achieves 2π at $24V_{\text{rms}}$. The induced birefringence (Δn_{ind}) of PS-BPLC can be described by the extended Kerr model [25] as

$$\Delta n_{\text{ind}}(E) = \Delta n_{\text{sat}}\{1 - \exp[-(E/E_S)^2]\}, \quad (4)$$

where Δn_{sat} stands for the saturated induced birefringence, E is the applied electric field, and E_S represents the saturation field. By substituting Eqs. (4) and (1) into Eq. (2), the phase change from n_i to n_o is obtained:

$$\delta = 4 \times \left(\frac{2\pi d \delta n}{\lambda}\right) = \frac{8\pi d \Delta n_{\text{sat}}}{3\lambda}\left\{1 - \exp\left[-\left(\frac{V}{dE_S}\right)^2\right]\right\}. \quad (5)$$

The PBS and reflective mirrors help to increase the optical path by 4×, since the vertical electric field (E) is uniform and is proportional to the applied voltage (V) as $E = V/d$. We fitted the experimental data with Eq. (5) and obtained good agreement, as plotted in Fig. 3(a). The fitting parameters are $\Delta n_{\text{sat}} = 0.0975$ and $E_S = 2.58$ V/μm. Therefore, the Kerr constant is 23.14 nm/V^2. In addition, to measure the response time of the PS-BPLC phase modulator, we replaced the CMOS camera in Fig. 2 with an iris and a photodetector. Then, we removed the biased voltage (~24 V) instantaneously at $t = 0$. The measured phase decay time (from 100% to 10%) is ~3.5 ms. Besides, the rise time (from 0% to 90%) is 0.96 ms with ~24 V, as Fig. 3(b) shows. Both response curves fit well with the double exponential equations described in [26]. Our LC host (JC-BP07N) has a very large $\Delta\varepsilon(> 300)$; that means the compound has several polar groups to obtain such a large Kerr constant [27]. A major tradeoff is increased rotational viscosity and slower response time. Due to small domain sizes, this response time is still more than one order of magnitude faster than that using a conventional nematic LC device.

At a given wavelength, the phase change is determined by the device structure, cell gap, and electric field as expressed in Eq. (5). When the cell gap decreases, the optical path length decreases linearly (here, $l = 4d$), but the electric field gets stronger. According to extended Kerr effect, the induced birefringence is proportional to E^2 in weak field region and then gradually saturates. Thus, the refractive index change (δn) gets larger as the cell gap decreases and, finally, achieves a saturation value. Therefore, there ought to be an optimal cell gap for achieving a certain phase change (say 2π). Figure 4 depicts the simulated $V_{2\pi}$ versus cell gap for PS-BPLC07 at $\lambda = 405$ (blue curve) and 633 nm (red), respectively. From fitting, we found $E_S = 2.58$ V/μm and $\Delta n_{\text{sat}} = 0.0975$ at $\lambda = 633$ nm. As depicted in Fig. 4, the minimum $V_{2\pi}$ at $\lambda = 633$ nm is 19.8 V with a cell gap $d = 6.84$ μm. Parameter E_S is independent of wavelength because, at a given temperature and voltage, the LC director reorientation profile is determined by the balanced elastic and electric torques; it has nothing to do with the probing wavelength. To obtain Δn_{sat} at a shorter wavelength, we measured the birefringence (Δn) of the LC host JC-BP07N at different wavelengths [28] and fitted the experimental data with a single-band birefringence dispersion model [29] as

$$\Delta n = G\frac{\lambda^2\lambda^{*2}}{\lambda^2 - \lambda^{*2}}, \quad (6)$$

where λ^* is the average resonance wavelength of the LC, and G is a proportionality constant. Excellent agreement is obtained with $G = 3.281$ μm^{-2} and $\lambda^* = 0.211$ μm (not shown here). The Δn_{sat} of PS-BPLC also follows the single-band birefringence dispersion model well with the same λ^*, but different G value (e.g., G') from the LC host [30]. By taking the ratio between Δn_{sat} and Δn of LC host at $\lambda = 633$ nm, we get $G' = 0.652$ μm^{-2} for PS-BPLC07. Therefore, Δn_{sat} at any wavelength can be calculated, and we find $\Delta n_{\text{sat}} = 0.120$ at $\lambda = 405$ nm. As λ decreases, $V_{2\pi}$ decreases because the required optical path length gets shorter while the LC birefringence gets higher. As Fig. 4 shows, the minimum $V_{2\pi}$ at $\lambda = 405$ nm is only ~10 V with an optimal cell gap $d \sim 3.57$ μm. Thus, $V_{2\pi}$ for the whole visible region is within the reach of LCoS, which enables the widespread application of BPLC spatial light modulators.

Based on Gerber's model [31], Kerr constant (K) is governed by Δn, $\Delta\varepsilon$, average elastic constant (k), and pitch length (p) of the BPLC as

$$K \sim \Delta n \cdot \Delta\varepsilon \cdot p^2/k. \quad (7)$$

From Eq. (7), employing an LC host with large Δn or large $\Delta\varepsilon$ is the most common way to boost Kerr constant [18,32]. In Fig. 3(a), we plotted the voltage dependent phase change for two blue phase materials with the same cell gap $d \sim 4.97$ μm.

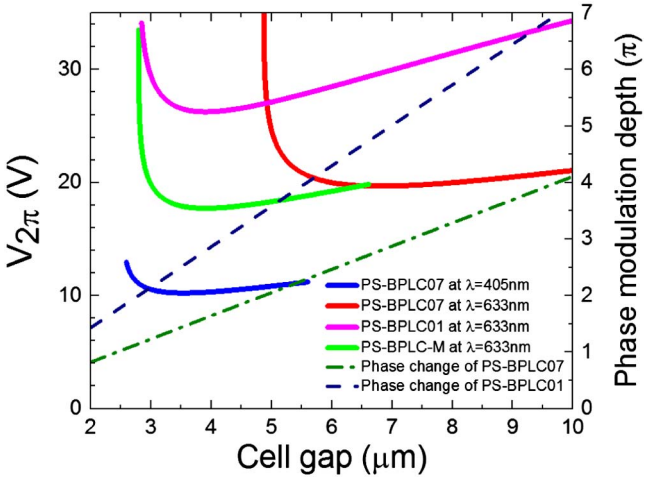

Fig. 4. Solid lines stand for simulated $V_{2\pi}$ versus cell gap for the specified BPLC materials; dashed lines represent the phase modulation depth vs. cell gap of PS-BPLC07 and PS-BPLC01 at $\lambda = 633$ nm.

Table 1. Physical Properties and Optimized Device Parameters for PS-BPLC Samples at $\lambda = 633$ nm

Sample	Δn_{sat}	Kerr Constant (nm/V^2)	Minimum $V_{2\pi}$ (V)	Cell Gap for Min $V_{2\pi}$ (μm)
PS-BPLC07	0.10	23.14	19.8	6.84
PS-BPLC01	0.17	7.46	26.3	3.94
PS-BPLC-M	0.17	16.41	17.7	3.91

For PS-BPLC07, its large $\Delta\varepsilon$ contributes to small E_S and large Kerr constant. The saturated birefringence is ~0.0975 at $\lambda = 633$ nm. Therefore, the phase change accumulates rapidly at a low voltage region and saturates gradually when the voltage exceeds ~25 V. The 2π phase change occurs at ~24 V. Also included in Fig. 3(a) is a different blue phase material PS-BPLC01 [18,23] with higher Δn_{sat} (~0.17 at $\lambda = 633$ nm), but smaller Kerr constant (~7.46 nm/V^2). The phase change of PS-BPLC01 does not saturate until $V \sim 70$ V, and the maximum phase change achieves 3.55π because of its larger E_S (~6 V/μm) and higher Δn_{sat}. The dielectric anisotropy of the LC host (JC-BP01N, JNC) is ~94 at low frequency. Although the Kerr constant of PS-BPLC01 is ~3× smaller than that of PS-BPLC07, its $V_{2\pi}$ (~27 V) is only 12.5% higher. The cell gap dependent $V_{2\pi}$ for PS-BPLC01 at $\lambda = 633$ nm is also included in Fig. 4. The minimum $V_{2\pi}$ (~26.3 V) is slightly higher than 24 V because of its smaller $\Delta\varepsilon$. As reported by Merck in [32], a BPLC host (designated as BPLC-M) with high Δn(~0.185) and large $\Delta\varepsilon$(~190) has been developed. To estimate the Kerr constant of PS-BPLC-M from Eq. (7), the other two parameters p and k need to be known as well. The pitch length can be controlled easily by changing the concentration of chiral dopants while the average elastic constant k is mainly determined by the compound structures of LC host. Let us assume the p^2/k of PS-BPLC-M is the same as that of PS-BPLC01; then the estimated Kerr constant of PS-BPLC-M is ~16.41 nm/V^2. Compared to the Δn of the LC host, the saturated birefringence (Δn_s) should decrease slightly because of the added chiral dopant and nonmesogenic monomer (~9 wt. % in total). Thus, its Δn_s is ~0.17 and $E_s \sim 4.05$ V/μm at $\lambda = 633$ nm. As shown in Fig. 4 (green curve), the minimum $V_{2\pi}$ is 17.7 V with $d \sim 3.9$ μm, which is even lower than that of PS-BPLC07 with a larger Kerr constant. This proves again that high birefringence plays an important role for lowering $V_{2\pi}$. In addition, the maximum phase modulation depth is determined by Δn_{sat}, λ, and d, as expressed in Eq. (5). We also plot the cell gap dependent phase modulation depth in Fig. (4) for PS-BPLC07 and PS-BPLC01 at $\lambda = 633$ nm, as the dashed lines show. The curve for PS-BPLC-M is the same as that of PS-BPLC01 since both have the same Δn_{sat} at $\lambda = 633$ nm. Therefore, the minimal operation voltage is achieved when the cell gap is slightly larger than that for 2π phase change.

In summary, we demonstrated a new device structure to allow a laser beam to traverse the BPLC layer four times in a reflective LCoS SLM. This novel approach exhibits several advantages. First, using a large Kerr constant polymer-stabilized BPLC07, the operation voltage is lower than 24 V in the entire visible region. Second, the response time remains fast (3 ms), which is at least 10× faster than a conventional nematic SLM. Third, PS-BPLC does not require any surface alignment layer so that the fabrication process is greatly simplified. Fourth, no extra substrate or bulky optical component is needed while multiplying the optical path by four times. As a result, the attractive features of LCoS, such as high resolution and light weight are preserved. Lastly, the new design helps suppress the fringing field effect of a high-resolution LCoS. Therefore, the proposed device structure opens a new door for widespread application of optically isotropic material-based SLM, including nano-sized polymer-dispersed liquid crystals.

Funding. Air Force Office of Scientific Research (AFOSR) (FA9550-14-1-0279).

REFERENCES

1. U. Efron, *Spatial Light Modulator Technology: Materials, Devices, and Applications* (Marcel Dekker, 1994).
2. S. Quirin, D. S. Peterka, and R. Yuste, Opt. Express **21**, 16007 (2013).
3. H. Ren and S.-T. Wu, *Introduction to Adaptive Lenses* (Wiley, 2012).
4. R. A. Forber, A. Au, U. Efron, K. Sayyah, S.-T. Wu, and G. C. Goldsmith II, Proc. SPIE **1665**, 259 (1992).
5. P. F. McManamon, T. A. Dorschner, D. L. Corkum, L. J. Friedman, D. S. Hobbs, M. Holz, S. Liberman, H. Q. Nguyen, D. P. Resler, and R. C. Sharp, Proc. IEEE **84**, 268 (1996).
6. F. Peng, Y. Chen, S.-T. Wu, S. Tripathi, and R. J. Twieg, Liq. Cryst. **41**, 1545 (2014).
7. F. Peng, Y. H. Lee, H. Chen, Z. Li, A. E. Bostwick, R. J. Twieg, and S.-T. Wu, Opt. Mater. Express **5**, 1281 (2015).
8. J. Yan, Y. Li, and S.-T. Wu, Opt. Lett. **36**, 1404 (2011).
9. R. W. Boyd, J. Leach, B. Jack, J. Romero, A. K. Jha, A. M. Yao, S. Franke-Arnold, D. G. Ireland, S. M. Barnett, and M. J. Padgett, Opt. Photonics News **21**(12), 48 (2010).
10. H. Toyoda, T. Inoue, N. Mukozaka, T. Hara, and M. H. Wu, SID Int. Symp. Digest Tech. Papers **45**, 559 (2014).
11. F. Peng, H. Chen, S. Tripathi, R. J. Twieg, and S.-T. Wu, Opt. Mater. Express **5**, 265 (2015).
12. F. Peng, D. Xu, H. Chen, and S.-T. Wu, Opt. Express **23**, 2361 (2015).
13. J. Sun, S.-T. Wu, and Y. Haseba, Appl. Phys. Lett. **104**, 023305 (2014).
14. H. Kikuchi, M. Yokota, Y. Hisakado, H. Yang, and T. Kajiyama, Nat. Mater. **1**, 64 (2002).
15. L. Rao, S. He, and S.-T. Wu, J. Display Technol **8**, 555 (2012).
16. R. M. Hyman, A. Lorenz, S. M. Morris, and T. D. Wilkinson, Appl. Opt. **53**, 6925 (2014).
17. S. A. Serati, X. Xia, O. Mughal, and A. Linnenberger, Proc. SPIE **5106**, 138 (2003).
18. L. Rao, J. Yan, S.-T. Wu, S.-I. Yamamoto, and Y. Haseba, Appl. Phys. Lett. **98**, 081109 (2011).
19. Y. Li, T. X. Wu, and S.-T. Wu, J. Display Technol. **5**, 335 (2009).
20. K.-H. Fan-Chiang, S.-T. Wu, and S.-H. Chen, J. Display Technol. **1**, 304 (2005).
21. J. Yan, Y. Xing, Z. Guo, and Q. Li, Opt. Express **23**, 15256 (2015).
22. M. J. Sansone, G. Khanarian, T. M. Leslie, M. Stiller, J. Altman, and P. Elizondo, J. Appl. Phys. **67**, 4253 (1990).
23. H.-C. Cheng, J. Yan, T. Ishinabe, and S.-T. Wu, Appl. Phys. Lett. **98**, 261102 (2011).
24. F. Peng, Y. Chen, J. Yuan, H. Chen, S.-T. Wu, and Y. Haseba, J. Mater. Chem. C **2**, 3597 (2014).
25. J. Yan, H.-C. Cheng, S. Gauza, Y. Li, M. Jiao, L. Rao, and S.-T. Wu, Appl. Phys. Lett. **96**, 071105 (2010).
26. D. Xu, J. Yan, J. Yuan, F. Peng, Y. Chen, and S.-T. Wu, Appl. Phys. Lett. **105**, 011119 (2014).
27. Y. Chen and S. T. Wu, J. Appl. Polym. Sci. **131**, 40556 (2014).
28. S.-T. Wu, U. Efron, and L. D. Hess, Appl. Opt. **23**, 3911 (1984).
29. S.-T. Wu, Phys. Rev. A **33**, 1270 (1986).
30. M. Jiao, J. Yan, and S.-T. Wu, Phys. Rev. E **83**, 041706 (2011).
31. P. R. Gerber, Mol. Cryst. Liq. Cryst. Sci. **116**, 197 (2011).
32. M. Wittek, N. Tanaka, D. Wilkes, M. Bremer, D. Pauluth, J. Canisius, A. Yeh, R. Yan, K. Skjonnemand, and M. Klasen Memmer, SID Int. Symp. Digest Tech. Papers **43**, 25 (2012).